Multi-Segmented Silicon Photonic Power Converters for Simultaneous Energy Harvesting and High-Speed Optical Wireless Communication

[1]Ch.Venkata Krishna Reddy, [2]J. Robert Adaikalaraj, [3]M. Muthuraj,[4]T. Priya, [5]Meruna P, [6]P. SatishKumar*

[1]Department of Electrical and Electronics Engineering, Chaitanya Bharathi Institute of Technology, Hyderabad.
[2]PG Department of Computer Applications, St. Joseph's College of Arts and Science (Autonomous), Cuddalore, Tamilnadu - 607001
[3]Department of Mechanical Engineering, NPR College of Engineering and technology, Natham, Dindigul, Tamilnadu
[4]Sree SaraswathiThyagaraja College, Pollachi, Tamilnadu - 642107
[5]Department of Medical Electronics, Sengunthar Engineering College, Thirunchengode, Tamilnadu, India.
[6]Department of Mechanical Engineering, Rathinam Technical Campus, Coimbatore, Tamilnadu, India - 641021

Email ID: [1]krishnareddy.chintala@gmail.com,[3]muthurajm@nprcolleges.org,[4]priyatsuriya@gmail.com, [5]merunaperumal@gmail.com, [6]spsatishkumar1986@gmail.com

Abstract

The energy-efficiency and speed of wireless communication, along with the rapid growth in the number of IoT devices, bring about the necessity to find the solutions that combine both power harvesting as well as optical reception to remove need to charge or replace batteries. Late-development has explored use solar cells receivers in high data detection. Photonic power converters silicon has6 times higher rates of electron movement than cadmium or silicon telluride cells and can be used in detecting data much faster and with higher power efficiency. However, they are limited junction capacitance raises with the active area, among data rate and power output. We design and test multi-segment Silicon based PPCs which can be used as energy collectors and data detectors. The capacitance and bandwidth is reduced by edge spacing active area at 2, 4 or 6 subcells, circle radius of 1, 1.5, or 2.08 mm, and increases the efficiency of light collection. The series-connected subcells are built on semi-insulating silicon substrate by etched trenches to provide isolation between subcells and minimizes the parasitic effects and increase absorption. The PPCs enabled a 1.5 m optical wireless communication, which is eye-safe, through adaptive bit and orthogonal frequency-division multiplexing and power allocation. The system was able to hit world record data of 3.5 Gbps, 4 times more than what had gone before it. The segmentation increases alignment sensitivity and the optical power beam is converted to 38.2% of the optical power by the device. The outcomeprovides new options to off-grid backhaul in future communication systems like 6G cellular systems.

***Keywords*:**Wireless communication**,** 6G, Photonics, Bandwidth, Power converters, Energy harvesting

1. INTRODUCTION

Demand of low latency, energy efficient and high-speedconnection accelerates the development of telecommunications on a worldwide level. The effect of lighting variation on silicon solar cell receivers in visible-light wireless communication was experimentally determined with regard to the industrial IoT. Findings indicate the sensitivity of performance to illumination, which can be used to rely on in 6G indoor network deployments [1]. A SWCNT/silicon heterojunction solar cell-based self-powered IoT sensing system made it

possible to use stable energy harvesting and wireless data transmission. The integration evidences the solar cells as small units of power in line with the photonic converter concepts of power of 6G devices [2]. An LSTM-based silicon solar cell visible-light positioning system recorded a mean error of 1.78 cm when using in the indoor wireless IoT. The strategy will make dense 6G environments more robust and will complement GaAs photonic power converters [3]. A low-cost silicon solar panel was shown, which was an optical wireless communication receiver that can receive energy and transmit data using DCO-OFDM and 28.3 Mb/s throughput with simultaneous energy collection and DCO-OFDM data transmission. The system was able to harvest 4.5 W and maintain the use of IoT devices and future 6G networks on the basis of solar cell-based photonic power converter frameworks [4]. CERN RadMon silicon-based system offers real-time radiation-monitoring with better reliability of distributed IoT systems based on wireless communication devices. Its modular architecture strengthens resilient silicon electronics infrastructure for next-generation high-density 6G environments [5].

Photonics 5/6G networks and IoT Photonic Photonic beamforming using silicon Photonic switches enabled 20 GHz bandwidth and 32 beam directions in a single photonic switched optical delay line beamformer [6]. A 16-bit embedded encryption system based on silicon was recommended in the safe wireless communication of wirelessly powered biomedical IoT devices. The streamlined PRINCE cipher lowers area and power, which allows safe data transfer in miniaturized 6G-activated photonic energy-harvesting structures [7]. A digital colorimetric sensor system that uses silicon photodiode was incorporated with wireless communication in a digital colorimetric sensor platform to monitor SO_2 real-time in smart energy systems. Remote sensing and consistent data transfer improve the green infrastructure with the help of the IoT-enabled architecture [8]. An implementation of a silicon-based synchronized pseudo-random number generator on a self-powered quantum tunneling timer was suggested in order to secure wireless IoT communication. It also allows the encryption to be tough without GPS synchronization in resource-constrained 6G environments using the low-power architecture [9]. Multi-junction InP/InGaAs photonic power converters engineered with the assistance of machine learning offered 15% better design efficiency and cost reduction in computational cost. The method enhances the production of photonic power converters using GaAs-based technology to facilitate power and data transmission systems concurrently [10].

The silicon PPC receiver which can achieve peak data throughput of 3.8 Gbps at same conditions: DCO-OFDM with adaptive bit and power loading to 1024-quadrature amplitude modulation (QAM). At a near-short-circuit operating point with load resistance of 950 0hms, at wavelength of 846 nm and optical transmitted power of 2.3 mW it was found that a pre-FEC BER of 1.610-3 (with 6.25 FEC overhead) was achieved. The device not only enables the high-speed receiving of signals but also converts segment of the incoming optical power up to 39.7% to useful electrical energy, a good example of an efficient concurrent optical-to-electrical power conversion and high-speed data detection with silicon technology. This advancement preconditions the future of energy-independent optical wireless communication systems make use of segmented silicon PPC architecture, which can work around the clock in an indoor and out of doors environment with limited maintenance needs and enhancing use of the wireless communication systems.

2. PROPOSED SYSTEM

2.1. Sample description

Experimental setup looks at utilization of silicon-based multi-segment photonic power converter as the receiver having 2, 4 and 6 segments at3 sizes namely S, M and L segments with active diameter 1 (S), 1.4 (M), and 2.11 mm (L) produced Fraunhofer ISE. Each subcell modules were electrically isolated by trenches cut in a semi-insulating silicon, using a metalinsulatormetal (MIM) isolation concept. Beyond the circular active area, there is etching done to expose lateral conduction layer that were located beneath the active silicon pn-junction. Polyimide filled docket metal bridges between adjacent circular sectors form a pizzalike design to create a series connected design to maximize output voltage and reduce effective capacitance. The polyimide-filled bridges electrically connect subcells in series while maintaining physical isolation, enabling voltage addition and effective capacitance reduction without introducing significant parasitic coupling.The micrograph of sample devices with the yellow and green sections depicting negative and positive contact point on front and rear side. The chips were mounted on wire bonded and planar submountelectrically to 2 larger contact pads at one side of chip. The front-side metal grid fingers collect photo-generated carriers in the silicon absorber layer and transfer electrons to metal busbars on periphery. At back of junction, tunnel diode was placed to reverse the polarity which allows lateral carrier movement between center and periphery under pn-junction through 5 μm-thick n-type silicon lateral layer to minimize series resistance and provide high speed response. Figure 1 represents a schematic layer structure.The intrinsic silicon bandgap (~0.74 eV) defines the long-wavelength absorption threshold, limiting efficient photogeneration beyond approximately 1200 nm. Operating near 850 nm ensures high quantum efficiency and optimal carrier generation while maintaining eye-safe operation and compatibility with common VCSEL sources.

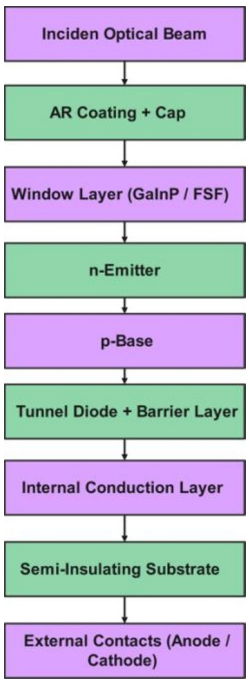

Fig. 1: Schematic illustration of multi-segment silicon receiver.

In this experimental case, a silicon-based multi-segment photonic power converter (PPC) serves as the receiver that is set in 2, 4, and 6 electrically isolated segments produced

in three active diameters of 1 mm (S), 1.4 mm (M), and 2.11 mm (L) by silicon-compatible processing on a semi-insulating substrate. The VCSEL produces a modulated optical beam that is incident on the segmented PPC in the system, with each circular subcell being isolated by trench etching and metal -insulator metal (MIM) structures and with polyimide-filled metal bridges linking neighboring sectors in a series pizzeria like configuration to boost output voltage and cut down effective junction capacitance. The silicon pn-junction structure comprises of a layer of absorber, measuring 3.65 0.4 mm, with surface passivation (SiO_2 / SiN stacks) to reduce surface recombination, a layer of n-doped front surface field, 400 nm, to allow movement of carriers at the lateral carrier-level without reducing transmittance at 850 nm and a bottom layer of conductor to reduce series resistance beneath the junction. The structures of tunnel junction allow the conversion of polarity and effective movement of carriers between central and peripheral areas. Grid fingers on its front side gather photogenerated carriers and direct them to peripheral busbars where they connect to the external receiver circuit through metallized anode and cathode contacts. The connected in series integrated segmented architecture increases the voltage across downstream circuitry, and at the same time reduces the overall device capacitance to the reciprocal capacitance rule, thereby reducing the bandwidthcapacitance trade-off and boosting the high-speed signal responsiveness in the free-space optical communication system.

Figure 2a shows that the spectrum responsivity curve has its highest point at 850 nm hence confirming the efficacy of the device under examination as a silicon-based photonic power converter (PPC). Strong response in this wavelength enables production of electrical power using normal near-infrared laser diodes and LEDs, which operate in the 850 nm range. It is the intrinsic bandgap of silicon (0.74 eV), determining the silicon long-wavelength absorption threshold, instead of the 881 nm, that causes the abrupt reduction of its responsivity at wavelengths above approximately 1200 nm. The spectral response recorded starts at approximately 400 nm, yet does not have any significance in the UV region (350 400 nm). The reduction in short-wavelength response is attributed to losses in the non-active surface layers, namely; the anti-reflection coating and strongly doped silicon front surface field area, not the GaInP window layer. This small difference between the experimental curve and the theoretical 100% quantum efficiency, denoted by the dotted reference line, could be explained by the insignificant optical and resistive losses such as partial shading of the front-side metallization grid and inefficiency of the anti-reflection coating. The close conformity of the experimental findings with the anticipated trend in the range of operating wavelengths is the evidence of high crystalline purity of the silicon absorber and adequate diffusion length of the minority carriers to collect the carriers. Moreover, Figure 2b shows the individual segment, and the summed currentvoltage (IV) characteristics of the light source of the series-connected six-segment system. The experiments were done under a steady 840 nm light with comparable, but not accurately quantified, optical irradiance levels.

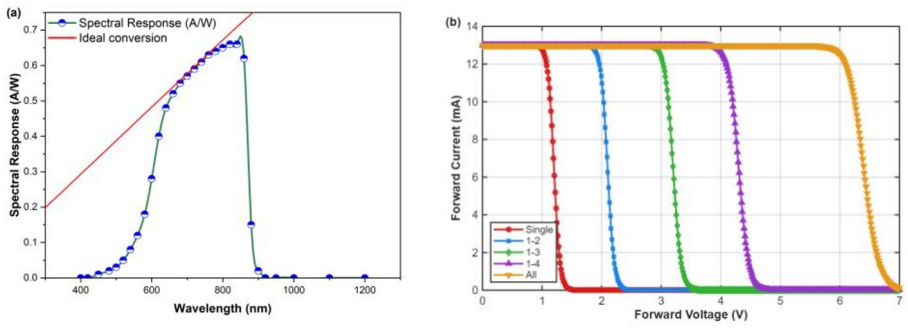

Fig. 2: a) Measured spectral response of single segment, b) I–V characteristics of segmented silicon device.

2.2. Experimental setup

The programmable DC power source were used to set up working point of the optical transmitter to provide a bias of 1.78 V and 6 mA to operate the 846 nm VCSEL in its linear modulation region. The same source is used in the DC characterisation of the silicon based PPC receiver which covers the illuminated and dark I-V characteristics. The Keysight M8195A arbitrary waveform generator is used to produce the OFDM-modulated electrical waveform used to measure system performance, like SNR and the possible throughput. The waveform of the AC generated is maintained at 1 V peak-to-peak, to avoid nonlinear distortion at VCSEL response. Discrete-time signal were produced by the OFDM signal of a pseudorandom binary slice with the frames produced by means of adaptive bit and power allocation depending on the parameter values as used in the reference work. The DC bias is added to AC-modulated signal using a bias-tee and the output drives the 846 nm VCSEL. The VCSEL wavelength emission is in the high responsivity region of the silicon photonic power converter, and results in a successful optical-to-electrical conversion of the converter. A dynamic allocation of modulation order and power levels to each subcarrier in the OFDM is done with an adaptive bit-loading and power-allocation method which dynamically determines the subcarrier's modulation order and power levels depending on the measured channel response. This flexible approach raises spectral efficiency and better utilization of bandwidth, thereby enabling the delivery of better data transmission by the changing connection conditions.

VCSEL source at 846 nm had produced a naturally divergent optical beam whose output power was 2.3 mW. The resulting radiation was then converted to parallel beam in the form of an aspheric collimating lens (Thorlabs ACL7560U-B) then proceeded a free-space distance of 1.5 m. The beam that was passed was collected and concentrated on the silicon-based multi-segment photonic power converter (PPC) receiver using a matching lens set. To minimize the outside electromagnetic and RF interference during high-speed measurements, the PPC receiver system was enclosed in a metallic shell. A simpler detector circuit was used to retrieve the analogue OFDM waveform, and in this case the silicon PPC was connected at parallel with variable RL to adjust electrical operating point and improve bandwidth trade-off. The load resistance was set to 0 -1 k to determine the best impedance regime around the short-circuit regime. A value of 950 0 was found to be optimal as an RL value to ensure that impedance was matched to the measurement electronics with the lowest reflections of the signal and minimum parasitics. When the device is used in close to short-circuit region, the effective junction capacitance is minimized and the silicon absorber carrier extraction is maximized and thus optimally transmits data rate.The selection of 850 nm is significant because it lies within the peak responsivity region of silicon, offers high modulation bandwidth capability, and ensures compatibility with mature VCSEL technology widely used in short-range optical communication systems.

The data characters of high-speed data connection are characterised with spectrum analyzer and 10 GHz real-time oscilloscope[11]. In communication research, the signal identified is then sent through a broadband RF amplifier (Mini-Circuits ZHL-42W+) and then digitized. This amplification step aims to amplify the signal amplitude, improve signal-to-quantization-noise ratio (SQNR), and reduce quantization noise added in process of analog-to-digital conversion of the oscilloscope to improve accurate demodulation of the OFDM waveform.A high-speed oscilloscope is essential to accurately capture the multi-GHz OFDM

waveform without aliasing or bandwidth limitation. Insufficient sampling bandwidth would underestimate system SNR and distort BER evaluation.

All recorded values of SNR are all at output of the RF amplifier stage. To boost the comparatively small signal generated by silicon-based PPC to the inherent noise floor of the measuring oscilloscope, a Mini-Circuits ZHL-42W+ broadband amplifier with a gain of 35.5 dB and noise figure of approximately 6.5 dB was used. Along with amplifying the fundamental signal, the amplification step increased the amplitude of the signal to be closer to the effective dynamic range of ADC of the oscilloscope, so effective number of bits (ENOB) was increased by about 6.4 (with no amplification) to about 7.0. The approach will ensure that the observed performance limitations are largely determined by the fundamental characteristics of the segmented silicon PPC receiver, as opposed to the limitations of the measuring device.The RF amplifier elevates the PPC output signal above the oscilloscope noise floor, improves effective dynamic range, and enhances the effective number of bits (ENOB), ensuring that measured performance reflects intrinsic device characteristics rather than instrumentation limitations.

2.3. OFDM communication

The implemented optical wireless communication system is used in DC-biased optical OFDM and channel estimation with M-ary QAM modulation, performed through the use of software in a personal computer with the help of MATLAB. The development of discrete-time OFDM waveform incorporates a systematic processing cycle that comprises of creation of pseudorandom binary sequence, adaptive assignment of bits and powers between subcarriers, M-QAM symbol mapping, inverse fourier transform and finally pulse shaping and oversampling. M-QAM modulation enables flexible spectral efficiency scaling by adapting constellation size according to channel SNR. Higher-order QAM was assigned to high-SNR subcarriers, maximizing total throughput while maintaining BER constraints.The resultant OFDM frame were fed arbitrary waveform generator, which converts it into optical modulation electrical signal in the form of a continuous-time analog signal. The analog OFDM waveform signal read at the silicon PPC receiver is sampled by a high speed oscilloscope at the receiver and then converted into the digital realm. The further signal processing in MATLAB is the synchronization followed by down-sampling, fast fourier transform (FFT) and matched filtering, as well as frequency domain equalization, M-ary QAM demodulation and channel estimation, to recover bit stream. In order to produce real-based time-domain OFDM signal suitable to be intensity modulated and directly measured (IM/DD), Hermitian symmetry of the subcarriers in the frequency domain is implemented, followed by the IFFT operation. Although there is the use of an FFT size of 1024, independent data are only transmitted by 511 subcarriers due to this symmetry constraint. An antenna MIMO based on graphene on a silicon dioxide substrate was designed and fabricated over semi-hexagons coloured with terahertz wireless communication. The small size enables 6G networks with high speed, Internet of Things, and sophisticated sensing platforms [12].

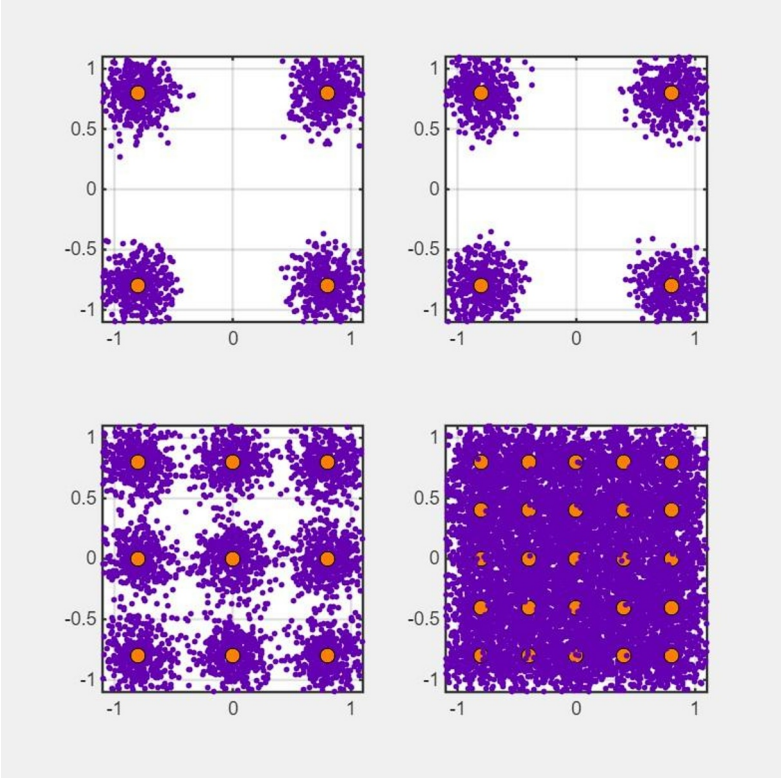

Fig. 3: SNR performance of PPC QAM receiver

Figure 4 (a, b, and c) shows experimentally obtained signal-noise ratio (SNR) profiles and the corresponding adaptive bit allocation when using a bit error rate 6.5×10^{-4} to achieve in the silicon-based PPC device with active d = 2.09 mm in 2, 4, and 6segment. A higher degree of segmentation increases the signal to noise ratio over a wider range of frequencies, enabling more bits to be allocated in each subcarrier of an OFDM system, thus increasing the overall data throughput. Two-segment silicon design is extremely nonperforming with SNR up to about 12 dB and a max of 3bits/subcarrier. The design based on four-segment silicon is much better and its SNR is 17 dB and it can be used up to 4 bits per subcarrier. These experiments confirm the fact that higher levels of segmentation in the silicon PPC can substantially reduce junction capacitance, widen electrical bandwidth and signal quality, and that this can be very important in spectral efficiency optimization and available data rate.

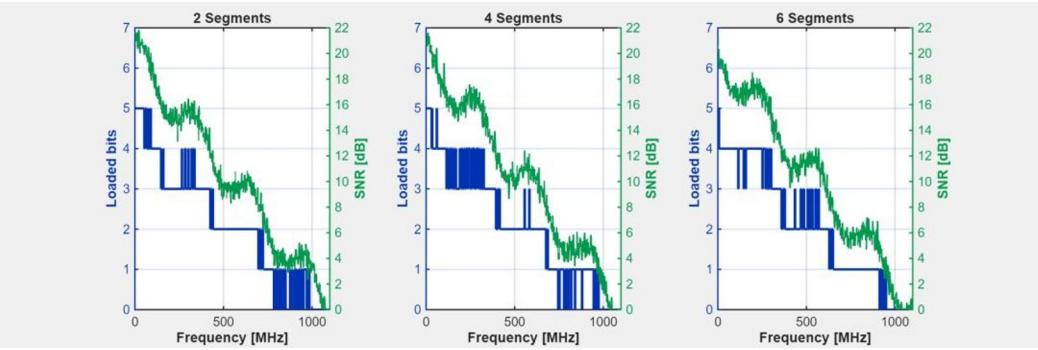

Fig. 4: a) Measured SNR with two-segment configuration, b) Measured SNR with four-segment configuration, c) Measured SNR with six-segment configuration.

3. RESULTS AND DISCUSSION

3.1. Experimental Results

An optical system of communication with a transmission distance of 1.5 m was developed to a free-space optical (FSO) system at 846 nm using a segmented silicon-based photonic power converter (PPC) as the receiver, and was able to allow simultaneous optical energy capture and high-speed data capture. The arbitrary waveform generator (AWG) is used to generate the RF modulation signal, which is applied with a DC bias current to the VCSEL within the linear modulation range in order to keep distortion to a minimum and optimize the overall signal to noise ratio (SNR) over the band of operation. The released optical beam travels through the free-space connection and falls on the segmented PPC, where it is transformed into an electrical signal with a load resistance of 950 Ω across a load of 950 Ω. The signal is then detected and operated by a receiver circuit through an amplifier, RF amplifier, and then analyzed with an oscilloscope and BER analyzer to check the performance of the circuit. The electrical-optical characterization of the laser establishes a distinct threshold behavior and a linear rise in optical power beyond threshold current, which makes the optical modulation to be stable and efficient and offers dependable transmission of data.

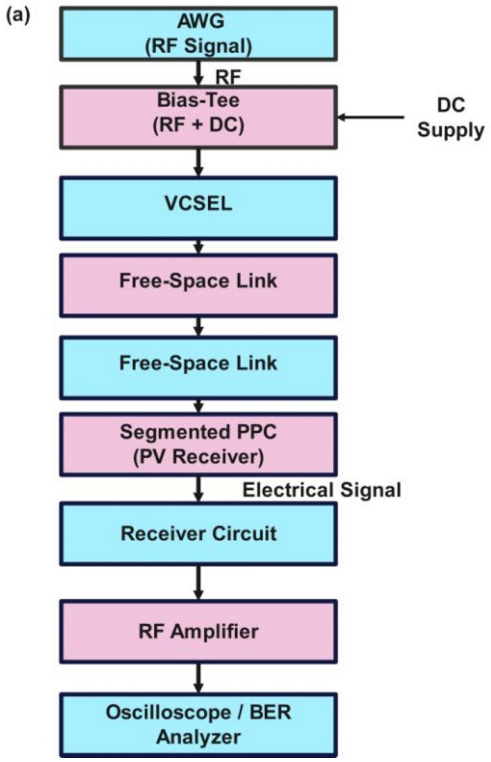

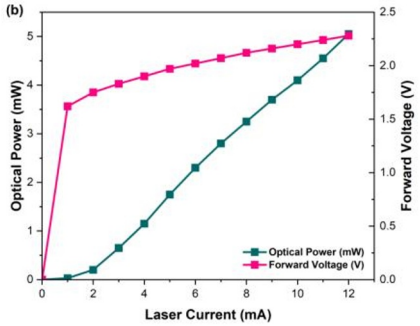

Fig. 5: a) Block diagram of silicon PPC receiver, b) Measured characteristics of VCSEL source;

The receiver end segmented silicon-based photonic power converter (PPC) is systematically evaluated by changing device dimension and the number of electrically isolated segments to achieve the best trade-off between efficiency of optical power collection and the speed of high-rate signal reception. The structural features obtained in the course of our research on the silicon devices developed before, allow the analysis of both the effect of junction capacitance in each of the silicon subcells, growing proportionately to the active area and the impact of the series connections of these subcells. A typical silicon PPC device is shown in figure and detailed manufacturing and structural data is given in the Sample Description section. SNR, achievable rate of data and BER determine the performance of the optical wireless link in different electrical working environments[13]. A parallel load resistance (RL) is obtained by integrating the observed illuminated I at V characteristics of each silicon sample in order to obtain the bias points. Running the PPC with a load resistance of 950.

In order to determine the fact that the performance limitations seen were due to the silicon-based PPC receiver design and not the optical source or the detecting electronics, the characteristics of the VCSEL were evaluated independently.

As shown in Figure 6a, the distribution of SNR was observed to be at the proximate circumstance of the receiver operating close to the short-circuit circumstance and the transmission bandwidth of the proposed connection. It was carried out using segmented silicon-based photovoltaic (PV) cells of 3 different diameters, 1.5 (M), 1 (S) and 2.08 mm (L), which had the total active areas of 1.0 mm, 1.4 mm and 1.7 mm. Each ofdevices was subdivided as 2, 4 or 6 electrically divided silicon subcells, individual segment between about 0.39 $mm^2$0.20 and 0.77 mm^2. The bandwidth of effective communication, which is actually the range of frequencies where the SNR is greater than 0 dB, was identified to increase with the number of segments, which implies that improved segmentation of the silicon architecture reduces effective capacitance of junctions and enhances response at high frequencies.

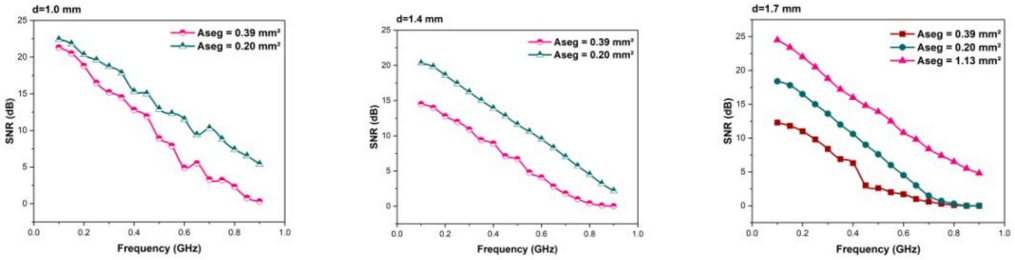

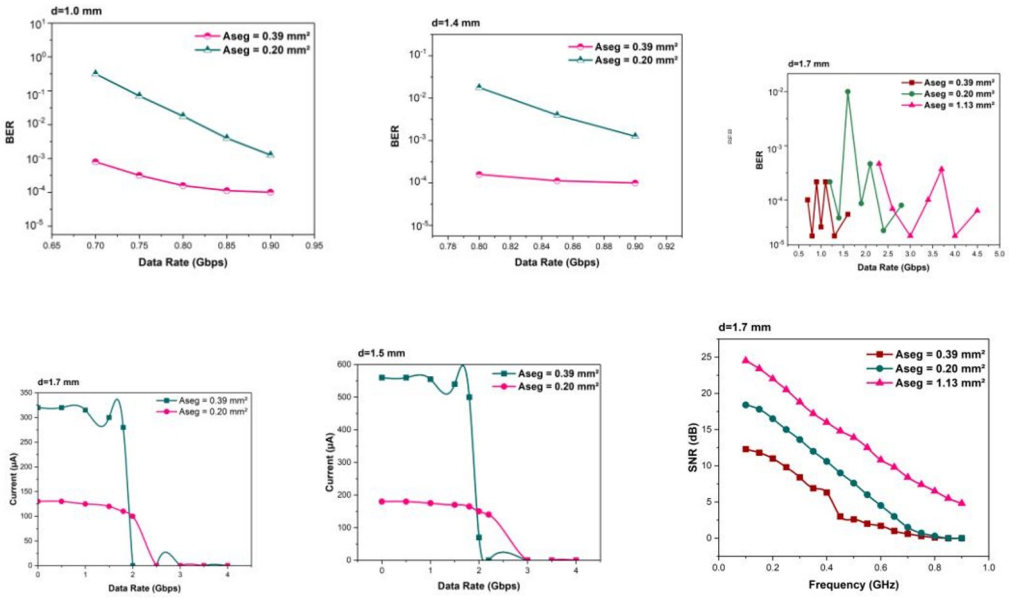

Fig. 6: a) Measured SNR versus segment number, b) BER versus data rate performance, c) PPC I–V characteristics under 2.3 mW.

It is observed that decreasing the effective segment area directly reduces the junction capacitance of each subcell. This reduction improves the RC time constant, extends the −3 dB bandwidth, enhances SNR at higher frequencies, and consequently increases the achievable OFDM data rate. Therefore, smaller segment areas provide superior communication performance, although at the expense of higher alignment sensitivity.The bandwidth of the 1.0 mm silicon PPC in the 2-segment (Aseg = 0.39 mm^2) and 4-segment (Aseg = 0.20 mm^2) configurations in the 2 segment and 4 segment with reduced segment area on the response of the RC-limited response was significantly greater, however, which is expected since the reduced segment area had a strong effect on the RC-limited response.The I–V characteristics determine the maximum power point (Pmp), photocurrent matching, and voltage scaling in segmented configurations. These parameters are critical for evaluating simultaneous energy harvesting and communication feasibility.

In the same way, the 1.4 mm silicon device also showed an increase in bandwidth of 0.77 GHz (2 segments, Aseg = 0.39 mm^2) to about 0.90 GHz (4 segments, Aseg = 0.20 mm^2).In the case of the 1.7 mm silicon PPC the bandwidth values of the 2, 4, and 6 segmented device were about 0.52 GHz, 0.78 GHz, and 0.95 GHz (Aseg = 1.13 mm^2, 0.39 mm^2, and 0.20 mm^2, respectively).The 6-segment layout provided the best bandwidth of almost 1 GHz which validated that more segmentation lowers the effective junction capacitance and improves high-frequency performance.Even though 6-segment silicon versions had been produced on the 1.0 mm and 1.7 mm devices, the full datasets were omitted, as the experimental requirements of the 1.0 mm and 1.7 mm devices included instability in mounting the devices and uneven illumination, which impacted repeatability.The omission of the full datasets does not compromise the validity of the reported trends, as the bandwidth enhancement with segmentation was consistently observed across repeatable measurements. However, quantitative repeatability analysis for those specific samples was limited due to mounting instability and spatial beam non-uniformity.

Figure 7 illustrates a scatter diagram of the PPC designs which are segmented on silicon, showing that the higher the number of segments, the lower the size of the area per

segment (mm^2) that it could achieve, the higher the attainable data rates would be. This action highlights the necessary trade-off between the capacitance of each silicon subcell junction, which decreases with area, and the overall improvement in performance provided by operation in series which is known as multi-segment operation. At the same time, we see that the SNR values are monotonically increasing with a higher degree of segmentation due primarily to reduced capacitive loading and increased high-frequency responsiveness as in Fig. 6c.

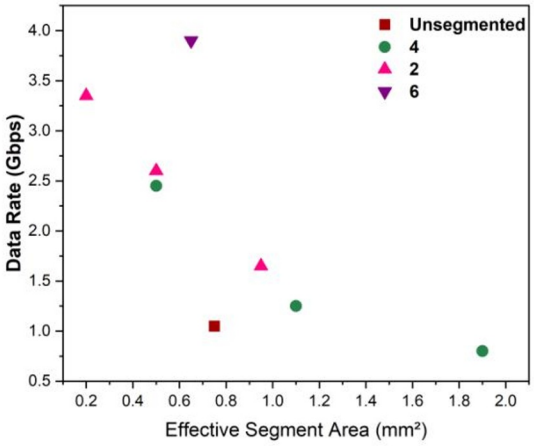

Fig. 7: Data rate versus effective segment area.

The currentvoltage characteristics of the segmented silicon photovoltaic (PV) cells, which are evaluated at an incident optical power of 2.1mW, represent electrical characteristics of the devices and indicate their possible power output and conversion efficiency in diverse segmentation arrangements. These plots demonstrate the change in the operating point maximum power point (Pmp) as a phenomenon of the individual segment area, the number of series-connected silicon subcells, and the overall device diameter, and ultimately, the energy captured. In order to reach the highest possible energy extraction, the external resistive load is tuned to synchronize electrical operating condition with Pmp, and therefore to maximise power transfer efficiency. The obtained values of power of two-segment silicon devices M(2), L(2) and S(2), are 0.89 mW, 0.89 mWand 0.49 mW, correspondingly. S(4), M(4), and L(4) in the four segment silicon design, M(4), L(4) and S(4), contribute to 0.59 mW, 0.67 mWand 0.39 mW,. The lowest output power is six-segment silicon device (L(6)) with lowest recorded output power was 0.11mW and this is attributed to non-uniform optical alignment and homogeneous spatial illumination as shown in Fig. 6c.The reduced output power in the six-segment configuration is primarily attributed to spatial photocurrent mismatch arising from slight optical misalignment and non-uniform beam distribution across the segmented surface. In future implementations, this limitation can be mitigated through beam homogenizers, micro-lens arrays, precision alignment stages, or expanded beam spot sizes to ensure uniform irradiance distribution.

In addition to measuring SNR, throughput and IV performance, the actual implementation of the segmented silicon based PPC receiver requires verification that the DC output obtained is able to provide power to the important front-end circuitry on a consistent basis. The existing setup of the laboratory has individually fed external bench devices (RF amplifier, oscilloscope, and PC-based digital signal processing), but not a fully integrated ultra-low-power system. The experiment thus substantiates the fundamental paramount

feasibility of multi-segment silicon PPCs to both simultaneously absorb optical energy and preserve multi-Gbps data acquisition. Under realistic short-range, high-SNR conditions, ultra-low-power front end receiver designs can operate at about 0.1 -0.2 mW, and 0.23 mW of the harvested power in 6-segment configuration is sufficient to transmit 3.8 Gbps, but larger platforms, like satellite systems or aerospace systems with larger photovoltaic apertures, can scale up the received power in line with that aperture. It is important to note that these values of harvested power are at the maximum power point; operating at the short-circuit condition to improve on the bandwidth reduces the output obtainable in DC and appropriate design margins must be added. Improved beam homogeneity and precise optical positioning has the potential to maximize energy harvesting and ease energy-independent working conditions. The degree of the photocurrent difference in series-connected silicon sections could be determined by the Imp/Isc ratio, but the power conversion efficiency (PCE) quantifies the optical-to-electrical conversion efficiency of different regions and different segmentation levels of the devices. The two-segment silicon cells have an Imp /Isc ratio of 96.2 % (0.79 mm 2), 99.5 % (1.77 mm^2), and 97.2 % (3.40 mm^2), which are equal to PCE values of 22.1, 38.7, and 39.7 %, respectively. The silicon versions with four segments exhibit reduced Imp/isc values of 85.0, 90.1, and 89.5 of the corresponding regions with the resultant PCE values of 19.8, 28.3 and 32.5. This 3.40 mm^2 six-segment silicon structure has the worst Imp/Isc ratio (66.1%), representing increased photocurrent mismatch that can be attributed to poor illumination or alignment, and thus the lowest PCE.

3.2. Analysis and Discussion

The increased level of silicon based photonic power converter (PPC) segmentation reduces the effective area that the silicon subcell occupies and consequently lowers the junction and parasitic capacitance of the silicon subcells and that of the series-connected system thereby allowing a more favorable response at high frequencies. The maximum experimentally achieved data throughput in this work was 3.5 Gbps under DCO-OFDM modulation with adaptive bit and power loading. Compared to earlier unsegmented silicon PPC-based SLIPT systems operating below 1 Gbps under similar optical power and wavelength conditions, this represents nearly a fourfold enhancement in data rate performance, confirming the effectiveness of the segmentation strategy in overcoming junction capacitance limitations.This tendency is empirically supported by the fact that the bandwidth of communication increases between 0.49 GHz and nearly 1 GHz as the 2-segment circuit is replaced with the 6-segment one in the largest silicon circuit (2.08 mm diameter). Data rate performance was validated through adaptive bit loading based on measured SNR profiles, BER verification using a pre-FEC threshold of 2.2×10^{-3}, and repeated waveform acquisition to ensure statistical consistency.Successful operation of the receiver to the short-circuit limit and efficient segmentation enhance carrier capture in the silicon junction, and promotes capacitive limits to reach a top data rate 3.5 Gbps, about 4 times high than previously reported silicon PPC-based systems operating under similar conditions. The findings show that segmentation and optimized parallel load resistance significantly improve bandwidth and signal-to-noise ratio (SNR), making multi-segment silicon PPC architecture a promising platform to implement compact eye-safe simultaneous lightwave information and power transfer (SLIPT) applications which require high data throughput. But further segmentation has other restrictions, in particular to energy sensitive systems, which need to be carefully controlled to maintain system efficiency.Non-uniform illumination leads to current mismatch among series-connected subcells, which limits the overall current to that of the lowest illuminated segment. Future experiments should incorporate spatial beam profiling and homogenization optics to ensure consistent irradiance across the active area and improve reproducibility.Increasing the number of segments reduces

the effective capacitance through reciprocal series connection, thereby extending bandwidth and improving SNR over a broader frequency range. This directly enables higher bit allocation per OFDM subcarrier and increases total throughput.

The I sub mp / I sub sc ratio of the segmented silicon based photovoltaic (PV) cell is that of current equivalence amongst the series connected subcells as regards optical energy conversion. When current matching currents are produced by both silicon segments, the same photocurrent is produced as a result, which requires the optical irradiance to be uniform across the entire active area; in this case the device can achieve power levels that are near the theoretical maximum. The silicon architecture with two segments has slightly increased the measured Imp/Isc values, which shows enhanced photocurrent equilibrium between segments. However, with the segmentation increased to four or six subcells, photocurrent generation differences across the series connection silicon segments occur due to spatial non-uniformities in illumination, which may be caused by distortions in beam profile, small optical misalignment, or partial shading of the overlay, effectively degrading current matching, the ratio of I<|human|>However, as the segmentation increases to four or six subcells, the spatial non-uniformities in the illumination give rise to differences in photocurrent generation in the series connected silicon segments, ultimately comprom. The efficiency degradation in the six-segment device is mainly caused by increased sensitivity to spatial non-uniformity. As segmentation increases, the probability of photocurrent mismatch rises, which reduces the overall power conversion efficiency despite improved bandwidth performance. A six-segment silicon PPC structure represents the greatest current mismatch present and the lowest PCE with the overall current of a series chain depressed by the segment with the lowest intensity. These works intimate that even though tighter segmentation results in a significant enhancement of communication bandwidth, and data throughput, it also increases sensitivity to illumination uniformity, and alignment, which are critical to successful energy harvesting. When very high data rates and high power efficiency are needed, such as in high-reliability applications such as aerospace platforms or remote sensing nodes, these results have demonstrated the importance of careful optical alignment methods or advanced beam homogenization schemes to achieve an effective tradeoff between communication performance and energy conversion efficiency. In prior research, silicon solar cell receiver with negative-bias offered 780 kHz bandwidth and 15.2 Mbps in underwater wireless communication. The system also captured energy, which will assist in IoT devices in subsequent 6GX photonic power converter systems [14].

A standard unsegmented silicon photovoltaic cell with a 0.78 mm^2 active area has a bandwidth of 125 MHz, supports a data rate of 522 Mbps, and achieves a power conversion efficiency (PCE) of 42, which is about 1.5 mW of incident optical power, making it suitable to compact and high speed receiver applications. A photovoltaic system based on organic PTB7:PC 7 1BM with a larger active area of 8 mm^2, on the other hand, has a lower data rate of 42 Mbps and an output power of 0.43 mW, which is more appropriate in low-power electronic systems. Similarly, large monocrystalline silicon panels (e.g., 3850 mm^2, 26% PCE) have reduced modulation bandwidths of approximately 9 MHz and related data rates of nearly 17 Mbps significantly, demonstrating that the design is more energy harvesting than communication-effective. The benchmarks reveal that the proposed multi-segment silicon-based PPC architecture can achieve higher high-speed communication throughputs with moderate sensitivity to optical alignment a slow degradation of PCE with higher segmentation. Therefore, the recreational use of applications with an interest in optimizing power economy can prefer fewer segments and even no segments of silicon design, but systems requiring higher bandwidth and throughput can benefit with more of those segments.

The use of vertically stacked multi-junction PPC designs with series connections but maintaining a unified aperture of the light absorber is also an option, but these designs show greater susceptibility to wavelength effects and thermo-optical effects, and might cause current imbalances between subcells. As reported in High-speed wireless communication A planar high-gain silicon cavity antenna attained 19 dBi at 275 GHz using a wide band. Its small size enables the short-range 6G connectivity and is complementary to the photonic power converter-based IoT systems [15].

Although additional versions of the devices were manufactured, they are said to be comprehensive and are not under the major focus of the research. In brief, the segmented silicon-based photonic power converter (PPC) architecture represents an important advancement in near-infrared optical wireless communications by effectively reducing the limitation of junction capacitance to achieve compact receivers that use a large bandwidth and enhance data rates at high data rates compared to the traditional unsegmented silicon cells. The segmentation approach allows each of the dynamics of optical absorption, carrier collection, and efficient parasitic capacitance to be optimized separately, providing design flexibility to application-specific applications to include high throughput backhaul communications or simultaneous lightwave information and power transfer (SLIPT) in energy-autonomous sensing systems.

4. CONCLUSION

This study illustrates effectiveness multi-segment silicon PPCs at SLIPT for energy-efficient, high-speed optical wireless communication. By dividing active region as 2, 4, or 6 cells, attained data throughput of 3.5 Gbps, signifying an estimated fourfold enhancement over the previous record of unsegmented silicon-based PPCs in analogous SLIPT systems. This constrained comparison presupposes DCO-OFDM modulation with adaptive bit/power loading, a pre-FEC BER of 2.2×10^{-3} (with 6.25% FEC overhead), near-shortcircuit operating points, 850 nm wavelengths, link distances of 1.0–1.7 m, and a maximum power conversion efficiency of 38.2% from 2.2mW input. Segmentation decreases capacitance, approaching 1 GHz for 2.11 mm cell by 6 segments, hence presenting photonic power convertor facilitators for 6G networks.

References

[1] C. I. D. V. del Valle Morales, J. C. T. Zafra, M. M. Morales-Céspedes, I. Martínez-Sarriegui, and J. M. Sánchez-Pena, “Exploring Bandwidth Capabilities of Solar Cells for VLC Applications,” *IEEE Trans. Industr. Inform.*, vol. 21, no. 1, pp. 894–901, 2025, doi: 10.1109/TII.2024.3468449.

[2] M. Parveen Banu, R. Jothilakshmi, S. Radha Rammohan, R. Vijay Anand, P. Anandan, and M. H. ALy, “Integration of 5G technologies for enhanced performance in optical network communication with channel allocation and reallocation,” *Opt. Quantum Electron.*, vol. 56, no. 6, 2024, doi: 10.1007/s11082-024-06808-7.

[3] L.-S. Hsu *et al.*, “Utilizing single light-emitting-diode (LED) lamp and silicon solar-cells visible light positioning (VLP) based on angle-of-arrival (AOA) and long-short-term-memory-neural-network (LSTMNN),” *Opt. Commun.*, vol. 524, 2022, doi: 10.1016/j.optcom.2022.128761.

[4] S. Das, A. Sparks, E. Poves, S. Videv, J. Fakidis, and H. Haas, "Effect of Sunlight on Photovoltaics as Optical Wireless Communication Receivers," *Journal of Lightwave Technology*, vol. 39, no. 19, pp. 6182–6190, 2021, doi: 10.1109/JLT.2021.3096734.

[5] K. Sangeetha, E. Anbalagan, R. Rajkumar, V. E. Pawar, and N. Muthukumaran, "Deep LSTM and Chi-Square Based Feature Selection Model for Traffic Congestion Prediction in Ad-Hoc Network," *Optical Memory and Neural Networks (Information Optics)*, vol. 34, no. 2, pp. 239–255, 2025, doi: 10.3103/S1060992X2570002X.

[6] C. Anuradha *et al.*, "A Robust Security System Using SHA-512 with Reinforcement Learning in Wireless Sensor Networks," *Engineering, Technology and Applied Science Research*, vol. 15, no. 6, pp. 30080–30086, 2025, doi: 10.48084/etasr.14048.

[7] S. Sarkar, J. Jiang, C.-Y. Tsui, and W.-H. Ki, "PRINCE Cipher and eFUSE-Based Embedded Encryption System for Optical Nerve Stimulator," *IEEE Sens. J.*, vol. 24, no. 19, pp. 30978–30993, 2024, doi: 10.1109/JSEN.2024.3439614.

[8] H. H. Cho *et al.*, "Digital colorimetric sensing for real-time gas monitoring for smart green energy system," *EcoMat*, vol. 5, no. 9, 2023, doi: 10.1002/eom2.12389.

[9] M. Rahman and S. Chakrabartty, "GPS-free synchronized pseudo-random number generators for internet-of-things," *Front. Comput. Sci.*, vol. 5, 2023, doi: 10.3389/fcomp.2023.1157629.

[10] R. F. H. Hunter *et al.*, "Machine learning enhanced design and knowledge discovery for multi-junction photonic power converters," *Sci. Rep.*, vol. 15, no. 1, 2025, doi: 10.1038/s41598-025-16408-4.

[11] E. I. Emon, A. M. Islam, M. S. Bashar, and A. Ahmed, "Design, fabrication, and performance analysis of a silicon solar cell integrated transparent antenna for wireless communications," *Engineering Science and Technology, an International Journal*, vol. 61, 2025, doi: 10.1016/j.jestch.2024.101915.

[12] R. H. Abd and H. A. Abdulnabi, "RECONFIGURABLE GRAPHENE-BASED MULTI-INPUT-MULTI-OUTPUT ANTENNA FOR SIXTH GENERATION AND BIOMEDICAL APPLICATIONS," *Journal of Engineering and Sustainable Development*, vol. 27, no. 6, pp. 798–810, 2023, doi: 10.31272/jeasd.27.6.10.

[13] R. Wang *et al.*, "Underwater Wireless Optical Communication Based on Flexible CIGS Solar Cells," *IEEE Photonics Technology Letters*, vol. 38, no. 2, pp. 65–68, 2026, doi: 10.1109/LPT.2025.3619403.

[14] W. Lei, Z. Chen, Y. Xu, C. Jiang, J. Lin, and J. Fang, "Negatively Biased Solar Cell Optical Receiver for Underwater Wireless Optical Communication System With Low Peak Average Power Ratio," *IEEE Photonics J.*, vol. 14, no. 4, 2022, doi: 10.1109/JPHOT.2022.3186702.

[15] M. S. Li, R. T. Ako, S. Sriram, C. Fumeaux, and W. Withayachumnankul, "Terahertz Planar Cavity Antenna Based on Effective Medium for Wireless Communications," *IEEE Trans. Terahertz Sci. Technol.*, vol. 14, no. 2, pp. 248–257, 2024, doi: 10.1109/TTHZ.2023.3338463.